

# Double Layer Structure of Ionic Liquids at the Au(111) Electrode Interface: An Atomic Force Microscopy Investigation

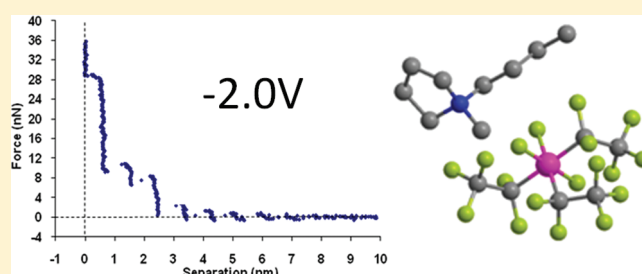
Robert Hayes,<sup>†</sup> Natalia Borisenko,<sup>§</sup> Matthew K. Tam,<sup>†</sup> Patrick C. Howlett,<sup>‡</sup> Frank Endres,<sup>§</sup> and Rob Atkin<sup>†,\*</sup>

<sup>†</sup>Centre for Organic Electronics, Chemistry Building, The University of Newcastle, Callaghan, NSW 2308, Australia

<sup>‡</sup>ARC Centre of Excellence for Electromaterials Science, Institute for Technology Research and Innovation, Deakin University, 221 Burwood Hwy, Burwood, VIC 3125, Australia

<sup>§</sup>Institute of Particle Technology, Clausthal University of Technology, Arnold-Sommerfeld-Str. 6, 38678 Clausthal-Zellerfeld, Germany

**ABSTRACT:** The double layer structure of two ionic liquids (ILs), 1-butyl-1-methylpyrrolidinium tris(pentafluoroethyl)trifluorophosphate ([Py<sub>1,4</sub>]FAP) and 1-ethyl-3-methylimidazolium tris(pentafluoroethyl)trifluorophosphate ([EMIm]FAP) at the polarized Au(111) electrode interface is probed using Atomic Force Microscopy force measurements. The force-separation profiles suggest a multilayered morphology is present at the electrified Au(111)–IL interface, with more near surface layers detected at higher potentials. At the (slightly negative) open circuit potential, multiple ion layers are present, and the innermost layer, in contact with the Au(111) surface, is enriched in the cation due to electrostatic adsorption. Upon applying negative electrode potentials (−1.0 V, −2.0 V), stronger IL near surface structure is detected: both the number of ion layers and the force required to rupture these layers increases. Positive electrode potentials (+1.0 V, +2.0 V) also enhance IL near surface structure, but not as much as negative potentials, because surface-adsorbed anions are less effective at templating structure in subsequent layers than cations. This interfacial structure is not consistent with a double layer in the Stern–Gouy–Chapman sense, as there is no diffuse layer. The structure is consistent with a capacitive double-layer model, with a very small separation distance between the planes of charge.



## INTRODUCTION

In recent years ionic liquids (ILs) have emerged as attractive solvents in electrochemistry (e.g., electrodeposition,<sup>1</sup> capacitors,<sup>2</sup> dye sensitized solar cells,<sup>3</sup> electrowetting,<sup>4</sup> etc.) because they are pure liquid electrolytes and therefore intrinsic conductors of electricity. ILs exhibit many performance advantages over conventional solvents in electrochemical settings.<sup>5–8</sup> For example, ILs can possess wide electrochemical and thermal windows, meaning that processes at extreme surface potentials or temperatures (respectively) can be conducted in ILs under conditions that are difficult or impossible to achieve using conventional solvents (usually aqueous electrolytes). Other important IL properties include low vapor pressure and the ability to dissolve both polar and apolar solutes. Notably, all of these solvent properties are tunable to a greater or lesser extent, insofar as the choice of anion/cation chemical structure controls the interionic forces that govern liquid behavior.

IL based electrochemical research is complicated by the absence of a comprehensive model for the structure of the electrified solid–IL interface and resulting potential distribution. Because a potential difference between the electrode surface and the bulk IL solution exists, a capacitive electrical double layer (ELD) must form, however the nature of the ion arrangements close to the interface is still a topic of debate. Some experiments have suggested a monolayer of adsorbed counterions<sup>9,10</sup> while

others imply an adsorbed ion layer plus an electrostatically bound diffuse layer.<sup>11</sup> In the absence of a clear understanding of the structure of this interface, fundamental electrochemical relationships, such as those described by the Butler–Volmer equation, cannot be applied in ILs.<sup>12</sup>

Classical descriptions of an aqueous ELD use mean-field models (e.g., Helmholtz,<sup>13</sup> Gouy–Chapman,<sup>14,15</sup> and Stern<sup>16</sup>). However these models are not applicable to ILs; aqueous electrolyte solutions consist mainly of neutral water molecules with some dissolved ions, whereas an IL is composed entirely of charged species. This means that the concentration of charged species at the interface will not differ greatly from the bulk. However, ion–ion and ion–surface interactions could be quite different in ILs because the ionic atmosphere is not diluted by the presence of a solvent, which leads to Debye lengths substantially less than the ion pair dimension; the Debye length is thus probably meaningless in an IL and electrostatic interactions are not appreciable over distances larger than the ion pair. Other concepts, such as the validity of IL ions as point charges may need to be re-examined because of their typically large, complicated shapes and charge delocalization. A model of the IL–electrode

Received: January 18, 2011

Revised: February 23, 2011

Published: March 17, 2011

interface will however incorporate some aspects of mean field theory, including the finite volume of ions, which sets the upper limit for the ion concentration at the electrode interface.<sup>17,18</sup>

IL interfaces are much more structured than those of molecular solvents,<sup>19,20</sup> so the ion arrangement at an electrode interface is expected to be rather different from that of aqueous electrolyte systems.<sup>18,21,22</sup> ILs are subject to a range of cohesive interactions (Coulombic, van der Waals, hydrogen bonding, solvophobic<sup>23</sup>), leading to well-defined structural organization at interfaces due to clustering of like molecular groups. Thus, three structurally distinct regions can be identified at IL interfaces:<sup>24</sup> the *interfacial* (innermost) layer that is composed of ions in direct contact with the second phase; the *bulk phase*, which refers to the bulk liquid region where structure depends on the degree of ion amphiphilicity;<sup>25</sup> and the *transition zone*, the region over which the pronounced interfacial layer structure decays to the bulk morphology. These definitions hold for all types of IL interfaces, including IL–air,<sup>26</sup> IL–liquid,<sup>27</sup> or (more importantly for this work) the solid–IL<sup>20</sup> interface.

Because solid surfaces impose rigid chemical and physical constraints on ions close to the interface, IL interfacial structure is most pronounced close to solid surfaces.<sup>20,24</sup> AFM experiments have examined IL structure in the interfacial layer and transition zones adjacent to a variety of solid substrates.<sup>20,28–31</sup> The interfacial layer has the greatest degree of organization and is enriched in cations that interact either electrostatically with anionic substrates or solvophobically with hydrophobic substrates. This innermost layer templates ion arrangements in the transition zone, which can extend up to five ion pair diameters from the interface. Oscillatory ion density profiles are detected in the transition zone. Similar findings have been reported by X-ray reflectivity studies at a charged sapphire surface.<sup>32,33</sup> To date, the structure adjacent to a cationic surface has not been investigated.

The structure of the IL–electrode interface has traditionally been inferred from capacitance measurements using electrochemical impedance spectroscopy (EIS). Many publications have employed this approach,<sup>11,34–41</sup> with values for the point of zero charge, double-layer thickness, and trends in ion adsorption behavior being reported. However, capacitance curves only provide averaged, macroscopic structural information about this interface since it is derived from the integral of ion profiles,<sup>7</sup> and there is considerable variation in published capacitance data. The appearance of capacitance curves for similar IL–electrode combinations range from pseudo-parabolic, to “bell-” and “camel-” shaped, each of which suggest different IL–electrode interface structure. As most authors do not seriously state the quality of their liquids<sup>42</sup> it remains an open question as to what extent these contradicting reports are due to impurities. At the very least, this complicates analysis and makes elucidating the ion arrangements from capacitance measurements challenging; Differences could suggest issues associated with IL<sup>43</sup> and electrode purity,<sup>11</sup> the frequency range of EIS measurements,<sup>11</sup> and hysteresis effects.<sup>36,37</sup> Therefore ILs cannot be treated as “just another solvent” for EIS measurements.

Theoretical descriptions of the IL–electrode interface have not kept pace with interest in ILs for electrochemistry, most likely due to the complexity of the IL–electrode interface and the many competing influences on ion arrangements. The mean field models of Kornyshev,<sup>18</sup> Oldham,<sup>21</sup> and Lauw et al.<sup>22</sup> represent the most advanced descriptions of the IL–electrode interface. In many respects, these models are analogous to Bikerman–Freise description of aqueous electrolytes<sup>44,45</sup> for the limiting case

where the solvent concentration is zero. Kornyshev’s model shows good agreement with experimental capacitance data and predicts both “camel-” and “bell-” shaped capacitance curves depending on the degree of ion compressibility at the interface (i.e., the density of ion packing). Lattice saturation effects were also proposed, and refer to the increase in double-layer thickness with higher surface potentials that result in decreased capacitance. Lauw et al. extend this to consider ion polarization close to the interface, such that as ions organize, the relative permittivity of the IL changes significantly as a function of distance from the interface.<sup>22</sup>

Molecular dynamics and Monte Carlo simulations can also be used to gain insight into the structure of the IL–electrode interface.<sup>46–49</sup> Within a few nanometers from the surface, distinct oscillations in charge density are predicted, corresponding to layered ion arrangements. For a generic IL cation with charged heads and neutral tails, a camel shaped capacitance curve is predicted due to ion adsorption and desorption at the interface.<sup>47</sup> However, current simulations generally underestimate specific IL–surface interactions as well as the potential for alkyl chain clustering that is observed in the bulk.<sup>25,50–53</sup> Thus, at uncharged surfaces these simulations predict no ordered IL layering, which is contrary to experimental findings.<sup>20,28</sup>

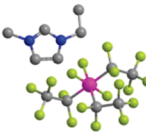
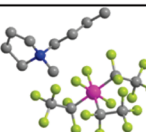
In this work, we employ Atomic Force Microscopy force curve measurements to elucidate the structure of the charged Au(111) electrode–IL interface. Until now, AFM experiments in ILs have only been conducted with surfaces at open circuit potential (ocp), but recent modifications to our AFM cell have enabled force curves to be obtained as a function of potential. This enables the double-layer structure of ILs to be probed. Data for two electrochemically useful (extremely pure) ILs, 1-butyl-1-methylpyrrolidinium tris(pentafluoroethyl)trifluorophosphate ([Py<sub>1,4</sub>]FAP) and 1-ethyl-3-methylimidazolium tris(pentafluoroethyl)trifluorophosphate ([EMIm]FAP) are presented at five surface potentials: open circuit potential (ocp), –1.0 V, +1.0 V, –2.0 V, and +2.0 V. These new results allow us to characterize the electrical double layer (EDL) structure of ILs and provide a new experimental framework for theoretical models.

## ■ EXPERIMENTAL SECTION

Samples of 1-butyl-1-methylpyrrolidinium tris(pentafluoroethyl)trifluorophosphate ([Py<sub>1,4</sub>]FAP) and 1-ethyl-3-methylimidazolium tris(pentafluoroethyl)trifluorophosphate ([EMIm]FAP) were purchased from MERCK as a custom synthesis in the highest available purity. Quality control measurements revealed all detectable impurities were below 10 ppm, with no hints of HF or oxides. Cyclic voltammetry, XPS, and in situ STM testing were also performed upon delivery at Clausthal to ensure the purity of the samples. Prior to use, the liquids were dried under vacuum at 100 °C to water contents well below 1 ppm (undetectable by Karl Fischer titration) and stored in a closed bottle in a desiccator (at Newcastle).

AFM force measurements were acquired continuously using a Digital Instruments NanoScope IIIa Multimode AFM with an E scanner in contact mode. The experiments were conducted in an incubator at 21 °C, as variation in temperature can influence IL interfacial structure.<sup>29</sup> The scan rate was 0.1 Hz while the vertical scan size was kept between 10 and 50 nm. One standard sharpened Si<sub>3</sub>N<sub>4</sub> tip cantilever (Digital Instruments, CA) was used for all experiments presented. The spring constant was measured to be (0.09 ± 0.005) N/m (thermal noise method).<sup>54</sup>

**Table 1.** Name, Abbreviation, Molecular Structure, Molecular Weight (MW), Density ( $\rho$ ), Molecular Volume (MV) and Ion Pair Diameter (D) of the ILs Used in This Work<sup>a</sup>

IL	Abbreviation	Structure	MW (g.mol <sup>-1</sup> )	$\rho$ (g.cm <sup>-3</sup> )	MV (nm <sup>3</sup> )	D (nm)
1-ethyl-3-methylimidazolium tris(pentafluoroethyl)-trifluorophosphate	Emim FAP		556.17	1.71	0.54	0.83
1-butyl-1-methylpyrrolidinium tris(pentafluoroethyl)-trifluorophosphate	[Py <sub>1,4</sub> ] FAP		587.27	1.45	0.67	0.89

<sup>a</sup> D is determined from ( $\rho$ ) assuming a cubic packing geometry according to the method described by Horn et al.<sup>19</sup> Carbon atoms are shaded gray, nitrogen are blue, fluorine are yellow, and phosphorous are pink. Hydrogens are not represented.

The tip was cleaned immediately prior to use by careful rinsing in Milli-Q water and irradiation with ultraviolet light for 40 min. The ILs were held in an AFM fluid cell, sealed using a silicone O-ring. These components were cleaned by sonication in Milli-Q water for 30 min, rinsed copiously in ethanol and Milli-Q water, and then dried using filtered nitrogen.

The AFM fluid cell setup was adapted to perform in situ electrochemical force measurements. This has enabled force–distance curves to be obtained as a function of applied surface potential. The changes made were inspired by a cell design of Wanless et al.<sup>55</sup> A thin cylindrical strip of Cu metal and 0.25 mm Pt wire were used as the counter electrode (CE) and “quasi” reference electrodes (QRE), respectively. The CE and QRE were cleaned first in dilute HCl acid solution and then washed and dried as per the AFM fluid cell and O-ring components. Atomically smooth Au(111) surfaces (a 300-nm thick gold film on mica) purchased from Agilent were used as both the working electrode (WE) and the solid substrate for AFM experiments. AFM imaging of the Au(111) substrates revealed a very low root-mean squared roughness value of 0.1 nm over a 300 nm<sup>2</sup> surface area. Thus, any differences in AFM force profiles observed can be ascribed to changes in surface potential and not underlying roughness.

The CE was mounted with the O-ring in the groove of the fluid cell. This established an equipotential WE surface because the CE's effective area is relatively large and axially symmetric with respect to the WE. The QRE was located directly above the center of the WE surface by securing the Pt wire through the outlet valve of the fluid cell. Ohmic loss was minimized by positioning the QRE to as close as possible (~2 mm) to the WE surface. The potential of all electrodes was controlled by an EG & G Princeton Applied Research Model 362 Scanning Potentiostat. The samples were held at each potential for 5 min prior to performing the force measurements.

The features of the force curves at a given surface potential did not alter over a 48-h period. Typical start distances for force scans were 30–50 nm from the Au(111) surface. The maximum applied force in contact was between 30 and 500 nN, however, no evidence of liquid structure was detected at forces greater than

30 nN in any system. Repeat experiments revealed that the number and period of the steps (oscillations) was constant. Every system and surface potential was studied over three or more separate experiments.

## RESULTS

AFM force–distance profiles for the two ILs 1-butyl-1-methylpyrrolidinium tris(pentafluoroethyl)trifluorophosphate ([Py<sub>1,4</sub>]FAP) and 1-ethyl-3-methylimidazolium tris(pentafluoroethyl)trifluorophosphate ([EMIm]FAP) (c.f. Table 1) are examined at five electrode potentials: open circuit potential (ocp), −1.0 V, +1.0 V, −2.0 V, and +2.0 V. The IL structure in both the innermost layer and the transition zone is commented upon from the force profiles obtained. Data for ocp is discussed first as it is relatively straightforward to interpret and can be compared with previous AFM experiments using similar ILs.<sup>20,31</sup> The results at ocp also provide a framework for understanding how IL structure changes at both positive (anodic) and negative (cathodic) electrode potentials, which will be addressed separately in the text. It is important to note the ocp is −0.16 V (vs Pt) for [Py<sub>1,4</sub>]FAP and −0.18 V (vs Pt) for [EMIm]FAP.

**Open Circuit Potential (ocp).** Figure 1A and 2A show force-separation profiles for an AFM tip approaching the Au(111) surface at ocp in [EMIm]FAP and [Py<sub>1,4</sub>]FAP, respectively. Using the data in Figure 1A as a guide, the AFM force profiles presented in this work can be interpreted as follows: Zero force is recorded beyond ~5 nm, because the AFM tip experiences negligible resistance moving through the bulk as it approaches the Au(111) surface. This shows that AFM is insensitive to any structure that might exist in the [EMIm]FAP bulk liquid. The tip encounters the first detectable layer at ~4.0 nm and pushes against it. 1.0 nN force is required to rupture this layer, and then the tip “jumps” 0.83 nm before encountering another layer at ~3.2 nm from the interface. The process is repeated a further three times with layers detected at 2.4, 1.6, and 0.8 nm, with the measured spacing of layers in excellent agreement with the predicted [EMIm]FAP ion pair diameter (0.83 nm) determined from the bulk density (c.f. Table 1). The magnitude of the push

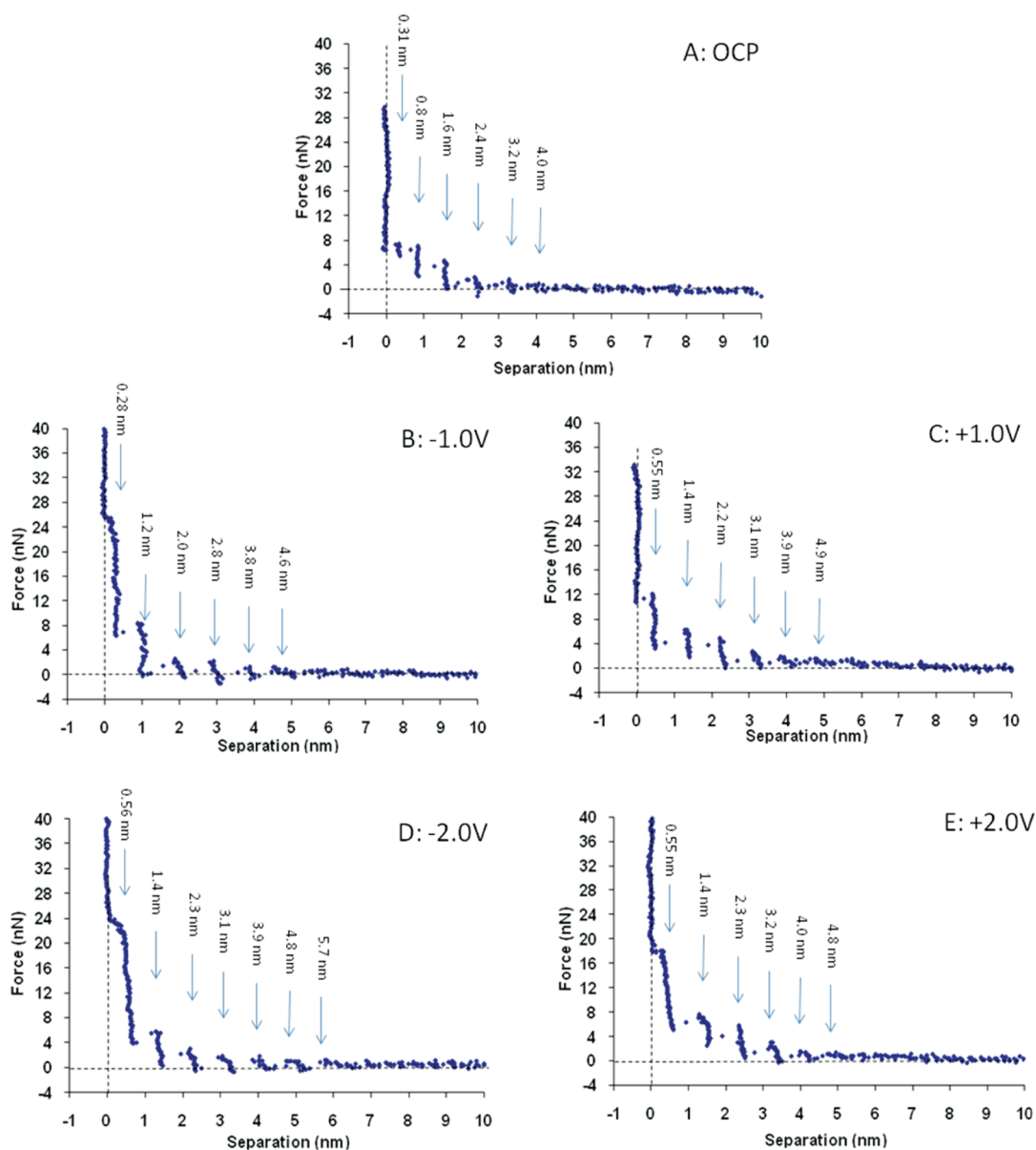


**Figure 1.** Typical force versus distance profile for an AFM tip approaching from a Au(111) surface in [EMIm]FAP at (A) Open Circuit Potential (ocp,  $-0.18$  V) (B)  $-1.0$  V (vs Pt) (C)  $+1.0$  V (vs Pt) (D)  $-2.0$  V (vs Pt) (E)  $+2.0$  V (vs Pt).

through forces for each ion pair layer increases as the tip moves closer to the surface. Consequently, the IL near surface structure is more pronounced closer to the Au(111) interface.

A key feature in Figure 1A is two small steps,  $0.5$  and  $0.3$  nm wide, detected nearest the interface. These step widths are substantially less than the [EMIm]FAP ion pair dimension ( $0.83$  nm), but their sum ( $0.50 + 0.30$ ) is consistent with the ion pair dimension. This suggests that the steps likely correspond to anion ( $0.50$  nm) and cation ( $0.30$  nm) sublayers, respectively. As it is likely that the Au(111) surface is negatively charged at ocp, electrostatics dictate that the  $0.30$  nm layer closest to the surface is enriched in cations. The next  $0.50$  nm step is likely an FAP anion layer, to quench the excess positive charge of surface adsorbed cations. Discrete cation and anion sublayers are detected because the cation is attracted more strongly to the surface than it is to the anion, such that the anion is displaced first, followed by the cation at slightly higher force. For layers at wider

separations, which are not in contact with the surface, the cations and anions are displaced by the AFM tip as ion pairs.

Well-defined near surface structure is also detected for [Py<sub>1,4</sub>]FAP at ocp (Figure 2A). At least four ion pair layers are observed in the force profile within the transition zone. There is also evidence that a fifth, weak layer is present given the absence of data points between  $4$  and  $5$  nm. The size of these ion pair spacings is  $0.9$  nm, consistent with the predicted [Py<sub>1,4</sub>]FAP ion pair diameter ( $0.89$  nm). An increasingly higher force is required to rupture layers closer to the interface as the IL is more structured closer to the Au(111) surface.

Interestingly, the rupture force is in every case greater for [Py<sub>1,4</sub>]FAP compared to [Emim]FAP. This is particularly evident for the innermost cation layers, at  $18$  and  $7$  nN, respectively. Similar to previous findings,<sup>20,31</sup> this result suggests that stronger surface-IL interactions are formed when the Coulombic charge on the ions is localized on one atom (c.f. [Py<sub>1,4</sub>]<sup>+</sup> cation) compared to delocalized



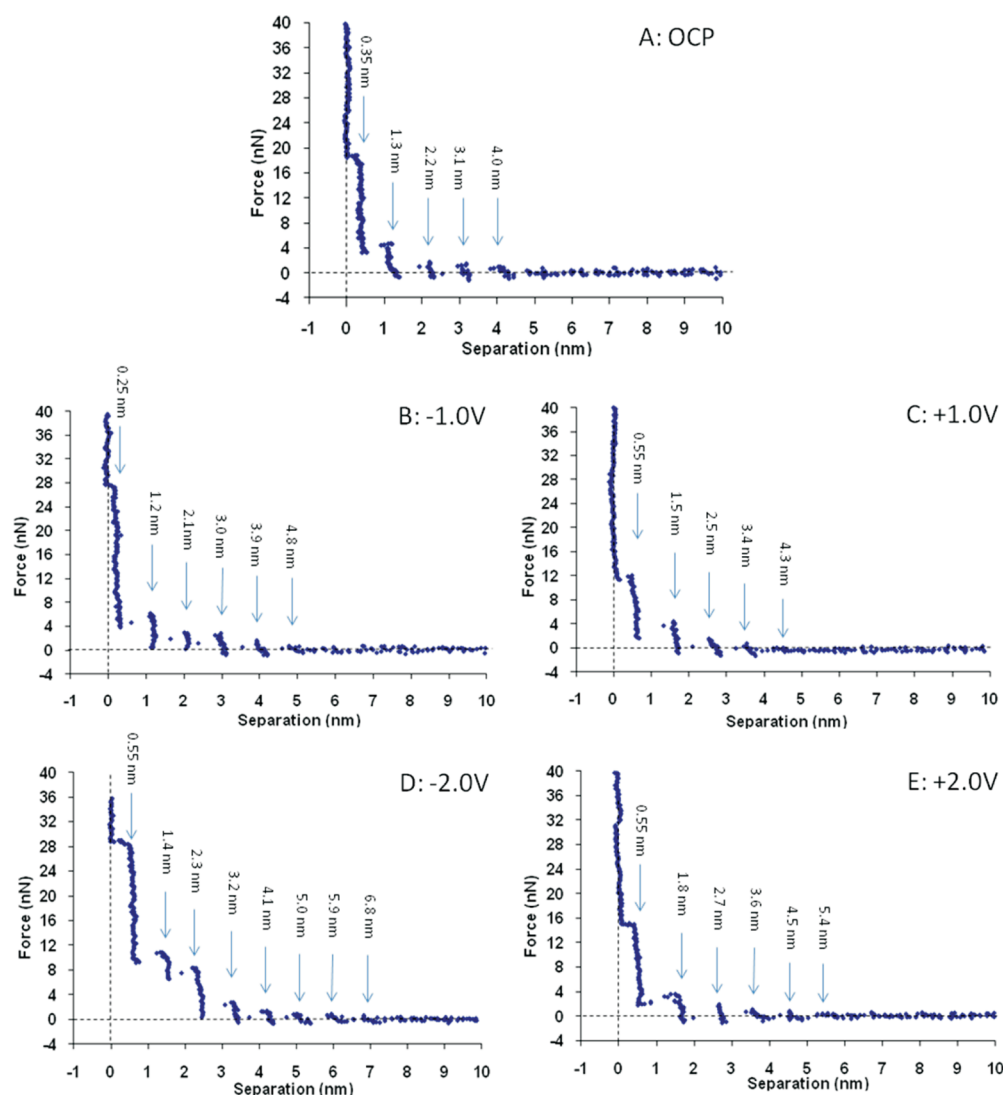


**Figure 2.** Typical force versus distance profiles for an AFM tip approaching from a Au(111) surface in [Py<sub>1,4</sub>] FAP at (A) Open Circuit Potential (ocp, -0.16 V) (B) -1.0 V (vs Pt) (C) +1.0 V (vs Pt) (D) -2.0 V (vs Pt) (E) +2.0 V (vs Pt).

across several atoms (c.f. [EMIm]<sup>+</sup> cation).<sup>31</sup> In a complementary publication, we demonstrate this mediates gold surface reconstructions in [Py<sub>1,4</sub>]FAP, including the famous herringbone structure.<sup>56</sup>

In Figure 2A, a small 0.35 nm step occurs closest to the surface. This step likely corresponds to an innermost layer enriched in [Py<sub>1,4</sub>]<sup>+</sup>. However, there is no small 0.5 nm anion layer detected subsequent to this; the next spacing in the profile is 0.9 nm, consistent with the size of an ion pair. This suggests a slightly different near-surface structure for [Py<sub>1,4</sub>]FAP. The longer cation alkyl chain for this IL means that solvophobic interactions become appreciable. Although the bulk structure for this IL has not been reported, a butyl chain on similar aprotic IL cations<sup>53</sup> is sufficiently amphiphilic to produce well-defined polar and apolar domains due to segregation of charged and uncharged molecular groups. At the Au(111) surface, an alternating polar and apolar layered arrangement should be maintained as solid interfaces serve to orient and align the pre-existing bulk IL structure.<sup>20</sup> The data in Figure 2A suggest that the order associated with this innermost cation layer decays to the bulk morphology over ~5 nm. This is likely to follow an alternating polar–apolar

arrangement of molecular groups, although significant interlayer mixing of ions is to be expected.

Significant changes in the force profiles are detected when a potential bias is applied to the Au(111) surface. This is noted for the size of the innermost layer, the size of the transition zone and the magnitude of the push through forces. In general, the data show that the ILs become more structured in response to an applied surface bias, particularly at negative potentials. This indicates that the electric field is inducing structure in the IL close to the electrode interface.

**Cathodic Electrode Potentials.** Data at -1.0 V and -2.0 V Au(111) electrode potentials are shown for [EMIm]FAP and [Py<sub>1,4</sub>]FAP in Figures 1B,1D and Figures 2B,2D, respectively. In the transition zone, steps appear sharper and better defined, and extend out over much larger distances from the interface. For [EMIm]FAP, five (at -1.0 V) and six (at -2.0 V) steps are detected at negative potentials, compared to four at ocp (-0.18 V). Likewise, [Py<sub>1,4</sub>]FAP shows four 0.9 nm steps at ocp (-0.16 V), whereas at -1.0 V and -2.0 V five and eight layers are clearly seen. Notably, the findings at -2.0 V for [Py<sub>1,4</sub>]FAP

are the most number of layers ever detected by AFM at the solid-IL interface, indicating a high degree of structure in this system.<sup>20</sup> These results demonstrate that the size of the transition zone, and consequently the extent of IL near surface structure, increases at more cathodic surface potentials; evidence of structure is first detected in [Py<sub>1,4</sub>]FAP out at 7 nm for −2.0 V, but only at 5 nm for ocp (−0.16 V). A similar effect is seen in [EMIm]FAP, where the onset of layering is seen at ~6 nm for −2.0 V, compared to 4 nm at ocp (−0.18 V).

In every instance, the magnitude of the push-through forces for corresponding layers is higher at −1.0 V than for ocp and likewise higher at −2.0 V than for −1.0 V. The variation in force is most evident in the innermost layer. In [Py<sub>1,4</sub>]FAP the rupture force of the innermost layer increases from 18 nN at ocp to 28 nN at −1.0 V. An even greater change is detected for [EMIm]FAP, which goes from 7 nN to 25 nN over virtually the same potential range. This shows that IL is more tightly bound to the surface upon applying a negative potential, leading to increased structure close to the interface.

When the electrode potential is increased from −1.0 V to −2.0 V, these innermost cation layers become so tightly bound that for both ILs the AFM tip cannot displace them from the surface. This is indicated by the size of the innermost step in Figures 1D and 2D. Steps 0.56 and 0.55 nm wide in [EMIm]FAP and [Py<sub>1,4</sub>]FAP are detected (respectively), consistent with the size of an anion sublayers in both cases. These detected anion layers require significantly more force to push through than any individual ion or ion pair steps at ocp. As the surface is strongly negatively charged, the innermost layer must be composed of cations, like that detected at ocp or −1.0 V. Thus, the “zero” separation in the −2.0 V force data corresponds to at least one strongly bound cation layer which the tip cannot penetrate. Because the absolute separation between tip and surface is not known in an AFM experiment, more than one undetected, strongly bound cation layer could be present at this potential.

The structure in the interfacial (innermost) layer is influenced by the applied electrode potential. Between ocp and −1.0 V, the width of the surface-adsorbed cation layer decreases from 0.35 to 0.25 nm in [Py<sub>1,4</sub>]FAP. For [EMIm]FAP a similar decrease might be present but the magnitude of the change (0.03 nm) is close to the error associated with the measurement. This indicates that the innermost cation layer flattens into a more compact orientation in response to a more negative electrode potential. Because the AFM tip is not able to probe the adsorbed cation layer for either IL at −2.0 V, it is not possible to comment on the orientation, although an even more compact flat arrangement may reasonably be expected.

Because interfacial layer structure is increased with higher cathodic potentials, the position of the subsequent steps in the transition zone can be shifted to larger tip–surface distances. This is illustrated in Figure 1A (ocp) and 1C (−1.0 V) in [EMIm]FAP, respectively. For example, the transition zone step positions at ocp are 0.8, 1.6, 2.4, 3.2, and 4.0 nm compared to 1.2, 2.0, 2.8, 3.8, and 4.6 nm at −1.0 V. At the higher surface potential, more electrostatic charge needs to be compensated for by the IL, leading to stronger cation adsorption in the innermost layer. Thus, an ion pair sized step is detected in the second layer at −1.0 V instead of an anion (seen at ocp), because enhanced cation adsorption induces an over-screening effect whereby subsequent ion layering overcompensates the electrostatic charge of the innermost layer. It is interesting to note that this effect was by and large not seen in the force profiles of [Py<sub>1,4</sub>]FAP at cathodic

potentials, which may be due to molecular effects such as the localization of charge on the cation and greater potential for solvophobic association between cation alkyl chains.

**Anodic Electrode Potentials.** Applying a positive potential to the electrode changes the force–distance profiles. Figure 1C,1E shows force–distance data at +1.0 and +2.0 V, respectively, for [EMIm]FAP. The corresponding data for [Py<sub>1,4</sub>]FAP at these surface potentials are presented in Figure 2C,2E.

Compared to negative biases, fewer ion pair layers are detected in the transition zone at positive surface potentials. In [EMIm]FAP, the first evidence of structure is observed 4.9 nm from the surface at both +1.0 V and +2.0 V, corresponding to five ion pairs layers. [Py<sub>1,4</sub>]FAP is similar with four (+1.0 V) and five (+2.0 V) layers measured. This suggests that a lower level of IL transition zone structure is present at positive surface potentials.

The innermost layers in each IL are thinner than the ion pair dimension (c.f. Table 1), and require moderately high force (~12 nN at +1.0 V and 15–18 nN at +2.0 V) to rupture. The positive potential of the surface dictates that this thin layer (0.55 nm) is enriched in anions for both ILs. This is the first time an interfacial (innermost) anionic layer at a solid interface has been detected by AFM. When the electrode potential is increased the rupture force increases, as per results obtained at negative potentials. Comparison of data obtained at positive potentials equal in magnitude but opposite in sign reveals that cations in the cathodic regime are more strongly adsorbed than anions in the anodic regime. This is likely a consequence of the FAP molecular structure in which the negative charge is delocalized over many fluorine atoms and somewhat shielded by the C<sub>2</sub>F<sub>5</sub> groups.

Interestingly, the interfacial layer at +2.0 V (Figures 1E and 2E), becomes slightly compressible, indicated by the nonvertical data for the innermost step. This is a result of molecular flexibility imparted by the fluorinated alkyl chains. Molecular flexibility on IL ions leads to fewer ion pair layers because flexible species can pack efficiently at interfaces without layering.<sup>57</sup> The present results show that FAP anions can also confer compressibility to the IL interfacial layers at high positive bias. Similar findings have previously been reported for IL cations.<sup>20</sup>

## DISCUSSION

The IL–electrified interface is complex. The force profiles obtained are very different from other molecular liquids or electrolyte solutions.<sup>58–60</sup> The key concept developed in this work is that the IL structure in both the innermost interfacial layer and transition zone evolves with the surface electrode potential, which in some respects parallels the multilayered structure of molten salts at an electrode interface.<sup>61–63</sup> However, there are some important physical and chemical differences between ILs and molten salts, which leads to subtle variation in the ELD structure. Firstly, by definition, IL ions are mobile at room temperature, meaning that they are capable of reorganizing themselves in response to changes in surface bias at ambient temperatures; no additional thermal energy is required to induce changes in IL interfacial structure. Moreover, unlike molten salts, IL anions and cations are never both spherical in geometry. The spherical shapes of molten salt ions enable them to pack like point charges in an electric field, forming neat alternating anion/cation layers that extend out from the interface. While some aspects of this model are clearly retained in ILs, the

unusual chemical structures of at least one, and often both, IL ions can impede neat ABABAB layered packing. Further many IL cations are surfactant-like in structure, consisting of distinct charged and uncharged regions, which can produce a locally layered sponge-like bulk structure that becomes more pronounced at interfaces.<sup>20</sup>

The interfacial layer of ions neutralizes the electric field of the Au(111) surface. As consequence, the interfacial layer should be composed of ions counter to the applied charge due to electrostatic interactions with the surface. The measured force profiles are consistent with this statement: at negative potentials, spacings consistent with the cation geometry, and vice versa, at positive surface potentials, anion-sized steps are observed. The negative ocp will likely produce an interfacial layer somewhat enriched in the cation.

The electric field controls the push-through forces for the innermost layer. By enhancing the electric field strength, the ion layer is held more tightly to the interface and consequently requires higher force for the AFM tip to displace.

Similarly, the orientation of ions in the interfacial layer is potential-dependent. For the cation, the reduced step size suggests that a flatter, more parallel ion-surface conformation is present at more negative potentials. The localization of Coulombic charge and the absence of an inflexible aromatic ring allow the  $[\text{Py}_{1,4}]^+$  cation to adopt a flatter surface orientation than  $[\text{EMIm}]^+$ . This results in the lower relative interfacial layer thickness for  $[\text{Py}_{1,4}]\text{FAP}$  at more negative potentials. In contrast, the FAP anion is a large ion with a  $C_3$  symmetry axis through the central phosphorus atom and Coulombic charge is delocalized across numerous fluorine atoms. This serves to weaken electrostatic adsorption of anions at positive potentials compared to the  $[\text{Py}_{1,4}]^+$  or  $[\text{EMIm}]^+$  cations. The size of the anion also means that it packs less effectively than the cations. These factors make inferring anion orientation in the interfacial layer difficult. One scenario is that at least two of the fluorinated alkyl chains anchor the anion at the surface, leading to the layer compressibility seen at +2.0 V potentials.

The orientation adopted by the ions in the innermost interfacial layer will maximize electrostatic attractions. Change in ion orientation as a function of surface charge is the origin of electrowetting phenomena in ILs,<sup>4,64</sup> and will find increased significance for manipulating flow behavior or confined structure in industrial settings.

Recent sum frequency spectroscopy (SFG) and electrochemical impedance spectroscopy (EIS) experiments suggest the IL electrical double layer is only one layer thick.<sup>9,10</sup> SFG was used to examine the composition and orientation of ions in the innermost layer. SFG spectra showed that at positive potentials anions are adsorbed at the interface and cations repelled, whereas negative potentials induced the imidazolium ring to adopt an orientation more parallel to the surface plane with anions repelled. The SFG results obtained are consistent with the structure inferred from AFM force-separation data in this work with one key difference: the IL electrical double layer must be more than one layer thick because near surface IL structure beyond the interfacial layer evolves with surface potential.

Significant structural changes are detected in the transition zone as a function of electrode potentials and thus the surface charge. The number of ion pair layers present reflects the surface charge of the Au(111) interface, with higher potentials leading to more near surface layers. This is particularly evident for cathodic surface potentials. Anodic surface potentials also yield more pronounced near surface structure than at ocp, however

molecular features of the FAP anion (size, charge delocalization and poor packing efficiency) reduces its ability to template subsequent ion layers in the transition zone. Data observed at cathodic potentials suggest that the comparatively small, flexible shapes of the IL cations, as well as the localization of electrostatic charge, enables the  $[\text{EMIm}]^+$  and  $[\text{Py}_{1,4}]^+$  species to pack efficiently at the electrode interface and template multiple ion pair layers into the transition zone. These trends are consistent with recent systematic capacitance measurements<sup>11</sup> which show a thicker double layer is generated at higher surface potentials.

The magnitude of the push-through forces increases substantially in the transition zone when a surface bias is applied, revealing the layered arrangement becomes significantly more ordered. This finding will impact upon applications including Lithium batteries<sup>65</sup> and dye-sensitized solar cells,<sup>3</sup> where the approach of dissolved  $\text{Li}^+$  ions or the redox couple (respectively) to the electrode interface could be impeded by increased solvent structure close to the interface. The increased capacitance of ILs containing  $\text{Li}^+$  (compared to the neat IL) has been suggested to be related to the well-known extension of the cathodic stability limit of these systems upon  $\text{Li}^+$  addition;<sup>66</sup> however, this may also result in low deposition rates once the  $\text{Li}^+$  ions present in the inner layer are consumed and the  $\text{Li}^+$  ions must diffuse to the electrode surface from the bulk electrolyte.

The AFM data presented in this work are consistent with an oscillatory potential distribution at the IL electrical double layer with a period equal to the ion pair diameter and an amplitude that decreases with distance from the surface. The force data do not contradict Kornyshev's theory of lattice saturation behavior at high negative potentials,<sup>18</sup> but no evidence of this was observed in capacitance measurements at the  $[\text{Py}_{1,4}]\text{FAP}$ –Au(111) interface in a complementary work.<sup>56</sup> It is possible that the increased number of ion pair layers detected in the transition zone supports an overscreening effect where individual ion sublayers overcompensate for the charge of the previous layer. Thus, with greater bias applied to the Au(111) surface, more electrostatic charge needs to be compensated for by the IL, leading to the increased number of layers.

Because the transition zone is composed of multiple ion pair layers a diffuse layer in the Gouy–Chapman–Stern sense cannot form in ILs. This casts doubt on the applicability of GCS models<sup>21</sup> for describing the structure at IL–electrode interfaces. The oscillatory nature of the ion arrangements means that successive ion pair layers near the surface cannot be considered as a discrete region that responds uniformly to changes in applied surface potential. Instead, ion pair layers respond as a function of their separation from the interface as small planes of charge over which the potential decays sinusoidally.

To our knowledge, this is also the first time structural, oscillatory forces<sup>67</sup> at the solid liquid interface have been directly measured as a function of electrode potential. While spectroscopic<sup>68,69</sup> or scattering<sup>70,71</sup> studies in aqueous systems have suggested that the near surface liquid structure changes in response to an applied potential bias, detection via surface force measurements has been made difficult by the presence of strong electrostatic and/or van der Waals DLVO forces, both of which are effectively screened in the IL.

## CONCLUSIONS

AFM was used to examine the IL electrical double layer structure at a Au(111) electrode surface. Ion arrangements vary



significantly as a function of applied potential, with more structure detected at higher voltages. The force–separation data obtained cannot be explained by a Stern–Gouy–Chapman double-layer model, as there is no diffuse layer in the conventional sense. The data suggest a capacitive double layer is present in ILs, with an oscillating potential decay profile and a very small separation distance between each plane of charge.

The innermost layer is enriched in ions that interact electrostatically with the surface. This layer contracted and became harder to displace as the surface potential was increased. Multiple ion pair layers were detected extending from the Au(111) surface. The number of layers depends on the applied potential, with larger applied potentials leading to more layers. This points to a templating effect at the IL–interface: higher surface potentials result in stronger electrostatic interactions with the innermost layer. This produces a more enriched, more tightly bound and more compact ion layer closest to the surface. This in turn induces neater packing in the next ion layer, and so forth, resulting in increased structure. The smaller size, localization of Coulombic charge, and reduced distance between the plane of ion–Au(111) surface charges mean that surface-adsorbed cations can induce more near surface structure than surface-adsorbed anions. This shows that the degree of structure at IL–electrode interface can be tuned by the surface potential and by the molecular structure of the IL ions. These AFM results further show that IL interfacial structure/properties can be designed for electrochemical interfaces, which will be exploited in many areas of IL research.

## AUTHOR INFORMATION

### Corresponding Author

\*E-mail: Rob.Atkin@newcastle.edu.au.

## ACKNOWLEDGMENT

This work was financially supported by an Australian Research Council Discovery Project (DP0986194) and the Deutsche Forschungsgemeinschaft (DFG) within the Priority Program SPP 1191–Ionic Liquids. The Newcastle group thanks Dr. Oliver Werzer and Mr. Timothy Murdoch for assistance with electrochemical measurements as well as Assoc. Prof. Scott Donne for the loan of a potentiostat. R.H. thanks the University of Newcastle for a PhD stipend.

## REFERENCES

- (1) Endres, F. *ChemPhysChem* **2002**, *3*, 144.
- (2) Ohno, H. *Electrochemical Aspects Ionic Liquids*; John Wiley & Sons, Inc.: New York, 2005.
- (3) Gorlov, M.; Kloos, L. *Dalton Trans.* **2008**, 2655.
- (4) Millefiorini, S.; Tkaczyk, A. H.; Sedev, R.; Efthimiadis, J.; Ralston, J. *J. Am. Chem. Soc.* **2006**, *128*, 3098.
- (5) MacFarlane, D. R.; Forsyth, M.; Howlett, P. C.; Pringle, J. M.; Sun, J.; Annat, G.; Neil, W.; Izgorodina, E. I. *Acc. Chem. Res.* **2007**, *40*, 1165.
- (6) Armand, M.; Endres, F.; MacFarlane, D. R.; Ohno, H.; Scrosati, B. *Nat. Mater.* **2009**, *8*, 621.
- (7) Su, Y.-Z.; Fu, Y.-C.; Wei, Y.-M.; Yan, J.-W.; Mao, B.-W. *ChemPhysChem* **2010**, *11*, 2764.
- (8) MacFarlane, D. R.; Pringle, J. M.; Howlett, P. C.; Forsyth, M. *Phys. Chem. Chem. Phys.* **2010**, *12*, 1659.
- (9) Baldelli, S. *J. Phys. Chem. B* **2005**, *109*, 13049.
- (10) Baldelli, S. *Acc. Chem. Res.* **2008**, *41*, 421.
- (11) Lockett, V.; Horne, M.; Sedev, R.; Rodopoulos, T.; Ralston, J. *Phys. Chem. Chem. Phys.* **2010**, *12*, 12499.
- (12) Buzzeo, M. C.; Evans, R. G.; Compton, R. G. *ChemPhysChem* **2004**, *5*, 1106.
- (13) von Helmholtz, H. L. *Wied. Ann.* **1879**, *7*, 337.
- (14) Gouy, G. *Compt. Rend.* **1910**, *149*, 654.
- (15) Chapman, D. L. *Philos. Mag.* **1913**, *25*, 475.
- (16) Stern, O. *Z. Elektrochem.* **1924**, *30*, 508.
- (17) Eigen, M.; Wicke, E. *J. Phys. Chem.* **1954**, *58*, 702.
- (18) Kornyshev, A. A. *J. Phys. Chem. B* **2007**, *111*, 5545.
- (19) Horn, R. G.; Evans, D. F.; Ninham, B. W. *J. Phys. Chem.* **1988**, *92*, 3531.
- (20) Hayes, R.; Warr, G. G.; Atkin, R. *Phys. Chem. Chem. Phys.* **2010**, *12*, 1709.
- (21) Oldham, K. B. *J. Electroanal. Chem.* **2008**, *613*, 131.
- (22) Lauw, Y.; Horne, M. D.; Rodopoulos, T.; Leermakers, F. A. M. *Phys. Rev. Lett.* **2009**, *103*, 117801.
- (23) Ray, A. *Nature* **1971**, *231*, 313.
- (24) Hayes, R.; Wakeham, D.; Atkin, R. *Ionic Liquid Interfaces*. Accepted for publication in *Ionic Liquids: COILED for Action*; Seddon, K. R., Rogers, R. D., Plechkova, N., Eds.; Wiley: New York, 2010.
- (25) Hayes, R.; Imberti, S.; Warr, G. G.; Atkin, R. *Phys. Chem. Chem. Phys.* **2011**, *13*, 3237.
- (26) Santos, C. S.; Baldelli, S. *Chem. Soc. Rev.* **2010**, *39*, 2136.
- (27) Iwahashi, T.; Sakai, Y.; Kanai, K.; Kim, D.; Ouchi, Y. *Phys. Chem. Chem. Phys.* **2010**, *12*, 12943.
- (28) Atkin, R.; Warr, G. G. *J. Phys. Chem. C* **2007**, *111*, 5162.
- (29) Wakeham, D.; Hayes, R.; Warr, G. G.; Atkin, R. *J. Phys. Chem. B* **2009**, *113*, 5961.
- (30) Hayes, R.; El Abedin, S. Z.; Atkin, R. *J. Phys. Chem. B* **2009**, *113*, 7049.
- (31) Atkin, R.; El Abedin, S. Z.; Hayes, R.; Gasparotto, L. H. S.; Borisenko, N.; Endres, F. *J. Phys. Chem. C* **2009**, *113*, 13266.
- (32) Mezger, M.; Schroder, H.; Reichert, H.; Schramm, S.; Okasinski, J. S.; Schoder, S.; Honkimaki, V.; Deutsch, M.; Ocko, B. M.; Ralston, J.; Rohwerder, M.; Stratmann, M.; Dosch, H. *Science* **2008**, *322*, 424.
- (33) Mezger, M.; Schramm, S.; Schroder, H.; Reichart, H.; Deutsch, M.; De Souza, E. J.; Okasinski, J. S.; Ocko, B. M.; Honkimaki, V.; Dosch, H. *J. Chem. Phys.* **2009**, *131*, 094701.
- (34) Alam, M. T.; Islam, M. M.; Okajima, T.; Ohsaka, T. *J. Phys. Chem. C* **2007**, *111*, 18326.
- (35) Nanjundiah, C.; McDevitt, S. F.; Koch, V. R. *J. Electrochem. Soc.* **1997**, *144*, 3392.
- (36) Lockett, V.; Sedev, R.; Ralston, J.; Horne, M.; Rodopoulos, T. *J. Phys. Chem. C* **2008**, *112*, 7486.
- (37) Druschler, M.; Huber, B.; Passerini, S.; Roling, B. *J. Phys. Chem. C* **2010**, *114*, 3614.
- (38) Lauw, Y.; Horne, M. D.; Rodopoulos, T.; Nelson, A.; Leermakers, F. A. M. *J. Phys. Chem. B* **2010**, *114*, 11149.
- (39) Alam, M. T.; Islam, M. M.; Okajima, T.; Ohsaka, T. *J. Phys. Chem. C* **2008**, *112*, 2601.
- (40) Alam, M. T.; Islam, M. M.; Okajima, T.; Ohsaka, T. *Electrochem. Commun.* **2007**, *9*, 2370.
- (41) Alam, M. T.; Islam, M. M.; Okajima, T.; Ohsaka, T. *J. Phys. Chem. C* **2008**, *112*, 16600.
- (42) Endres, F. *Phys. Chem. Chem. Phys.* **2010**, *12*, 1648.
- (43) Seddon, K. R.; Stark, A.; Torres, M. J. *Pure Appl. Chem.* **2000**, *72*, 2275.
- (44) Bikerman, J. J. *Philos. Mag.* **1942**, *33*, 384.
- (45) Freise, V. V. *Z. Elektrochem.* **1952**, *56*, 822.
- (46) Fedorov, M. V.; Kornyshev, A. A. *J. Phys. Chem. B* **2008**, *112*, 11868.
- (47) Fedorov, M. V.; Georgi, N.; Kornyshev, A. A. *Electrochem. Commun.* **2010**, *12*, 296.
- (48) Sha, M.; Wu, G.; Dou, Q.; Tang, Z.; Fang, H. *Langmuir* **2010**, *26*, 12667.
- (49) Vatamanu, J.; Borodin, O.; Smith, G. D. *J. Am. Chem. Soc.* **2010**, *132*, 14825.



- (50) Atkin, R.; Warr, G. G. *J. Phys. Chem. B* **2008**, *112*, 4164.
- (51) Greaves, T. L.; Kennedy, D. F.; Mudie, S. T.; Drummond, C. J. *J. Phys. Chem. B* **2010**, *114*, 10022.
- (52) Hardacre, C.; Holbrey, J. D.; Mullan, C. L.; Youngs, T. G. A.; Bowron, D. T. *J. Chem. Phys.* **2010**, *133*, 074510.
- (53) Triolo, A.; Russina, O.; Bleif, H. J.; DiCola, E. *J. Phys. Chem. B* **2007**, *111*, 4641.
- (54) Hutter, J. L.; Bechhoefer, J. *Rev. Sci. Instrum.* **1993**, *64*, 1868.
- (55) Wanless, E. J.; Senden, T. J.; Hyde, A. M.; Sawkins, T. J.; Heath, G. A. *Rev. Sci. Instrum.* **1994**, *65*, 1019.
- (56) Atkin, R.; Borisenko, N.; Drüschler, M.; El Abedin, S. Z.; Endres, F.; Hayes, R.; Roling, B. *Phys. Chem. Chem. Phys.* **2011**, accepted for publication.
- (57) Christenson, H. K. *J. Chem. Phys.* **1983**, *78*, 6906.
- (58) Butt, H.-J.; Cappella, B.; Kappl, M. *Surf. Sci. Rep.* **2005**, *59*, 1.
- (59) Cappella, B.; Dietler, G. *Surf. Sci. Rep.* **1999**, *34*, 1.
- (60) Warr, G. G. *Curr. Opin. Colloid Interface Sci.* **2000**, *5*, 88.
- (61) Sotnikov, A. I.; Esin, O. A. *Proc. of Third All-Soviet Conferences Khimia* 1966, Leningrad, 209.
- (62) Graves, A. D. *Electroanal. Chem.* **1970**, *25*, 349.
- (63) Graves, A. D. *Electroanal. Chem.* **1970**, *25*, 357.
- (64) Restolho, J.; Mata, J. L.; Saramago, B. *J. Phys. Chem. C* **2009**, *113*, 9321.
- (65) Howlett, P. C.; MacFarlane, D. R.; Hollenkamp, A. F. *Electrochem. Solid-State Lett.* **2004**, *7*, A97.
- (66) Yamagata, M.; Fukuda, Y.; Tanaka, R.; Ishikawa, M. *ECS Trans.* **2008**, *16*, 133.
- (67) Israelachvili, J. N. *Intermolecular and Surface Forces*; Academic Press: London, 1992.
- (68) Nihonyanagi, S.; Ye, S.; Uosaki, K.; Dreesen, L.; Humbert, C.; Thiry, P.; Peremans, A. *Surf. Sci.* **2004**, *573*, 11.
- (69) Noguchi, H.; Okada, T.; Uosaki, K. *Electrochim. Acta* **2008**, *53*, 6841.
- (70) Toney, M. F.; Howard, J. N.; Richer, J.; Borges, G. L.; Gordon, J. G.; Melroy, O. R.; Wiesler, D. G.; Yee, D.; Sorensen, L. B. *Nature* **1994**, *368*, 444.
- (71) Toney, M. F.; Howard, J. N.; Richer, J.; Borges, G. L.; Gordon, J. G.; Melroy, O. R.; Wiesler, D. G.; Yee, D.; Sorensen, L. B. *Surf. Sci.* **1995**, *335*, 326.